Melting and Misalignment of Solid Crystalline Krypton Inclusions in Aluminum

H. H. Andersen,[1] J. Bohr,[2] A. Johansen,[1] E. Johnson,[1] L. Sarholt-Kristensen,[1] and V. Surganov[1,a]

[1]*Physics Laboratory, H. C. Ørsted Institute, DK-2100 Copenhagen Ø, Denmark*

[2]*Physics Department, Risø National Laboratory, DK-4000 Roskilde, Denmark*

(Received 10 July 1987)

Ion-implantation–induced crystalline krypton inclusions in aluminum, epitaxially aligned with the matrix, have been investigated with x-ray diffraction and Rutherford-backscattering channeling analysis. The data show a dual size distribution of the krypton bubbles. In samples annealed up to 620 K and subsequently cooled, the larger bubbles melt in a pressure-broadened transition at 114–118 K. The smaller bubbles remain solid upon heating but, as a result of a roughening transition on the aluminum facets of the cavities, the Kr crystallites gradually lose their epitaxial alignment.

PACS numbers: 61.70.Qi, 64.70.Dv

The discovery in 1984 that implanted gas atoms trapped in bubbles formed after ion implantation of heavy inert gases into metals are in solid form[1-10] finally solved the question discussed for more than thirty years regarding the pressure in these bubbles: In order to confine solid precipitates of the noble gases at room temperature, the pressure must exceed 1–2 GPa. As a rule, the structure of the crystallized gas bubbles is fcc in an fcc matrix, and despite very large misfits, the bubbles are aligned epitaxially with the crystal lattice of the matrix.[3,7] *In situ* heating experiments in the electron microscope have shown melting of the bubbles, which upon cooling solidify in epitaxial regrowth.[8,10,11] Heating to higher temperatures, where the size of the bubbles increases considerably, reduces the pressure in the bubbles, and solidification, then occurring at cryogenic temperatures, can only partially fill the cavities.[8,10,11]

Nearly all the experiments on such solid inert-gas inclusions have up till now been carried out with the use of transmission electron microscopy and selected-area diffraction. In order to obtain quantitative information on the structure of the bubbles, we have carried out x-ray diffraction on aluminum single crystals implanted with krypton. This has been attempted previously under glancing-angle conditions,[12,13] where geometrical information alone was obtained. Aluminum single-crystal disks with a ⟨111⟩ normal were implanted at room temperature with 200- and 100-keV energy to fluences of 2×10^{20} m^{-2} and 1.5×10^{20} m^{-2}, respectively, to give average implant concentrations of 8–10 at.% in a layer with a thickness of $\simeq$150 nm. This is sufficient to produce a dense distribution of solid krypton bubbles aligned epitaxially with the aluminum matrix.[8] X-ray diffraction was carried out at high and low temperatures with Cu-$K\alpha$ radiation from a rotating-anode source. To obtain further information on the fate of the implanted krypton, the crystals were also investigated by Rutherford-backscattering analysis of channeled 1.5-MeV He^+ ions.

As-implanted crystals show distinct ⟨111⟩ krypton diffraction peaks which do not disappear after annealing to 620 K. At a temperature of 12 K, where all krypton particles are solid, the average krypton lattice parameter is 0.574 nm in both annealed and as-implanted samples. At room temperature the lattice parameter in an as-implanted crystal is 0.555 nm which, with the use of Ronchi's analysis,[14] corresponds to a pressure of 1.2 GPa. All the peaks are skewed with the steeper side at the smaller Q values. They can be fitted by a sum of two Gaussian distributions of different widths and slightly different positions. One represents small bubbles with an average size of 3.5 nm containing krypton under high pressure (e.g., small lattice parameter), and the other represents bubbles with an average size of 9 nm at a lower pressure. The sizes are estimated at $4(\pi\ln2)^{1/2}/\Delta q$, where Δq is the FWHM of the longitudinal peaks.

The diffraction peaks contain information from all the bubbles that are aligned epitaxially with the matrix. At 12 K the ⟨111⟩ peak from the annealed crystal is relatively narrow and has a large integrated intensity. The small width is due to an increased contribution from the larger-bubble fraction, originating from a slight bubble growth which is also seen in electron microscopy.[8] The larger integrated intensity of this peak comes from two different contributions. The annealing process causes melting of the larger bubbles and recovery of the damaged aluminum matrix. Upon cooling this leads to a better epitaxial regrowth of the bubbles. Furthermore, some interstitial krypton atoms (see below) become mobile upon annealing. They will be either trapped in already existing bubbles or lost at the surface.

Heating of the crystal, which has been annealed at 620 K and subsequently cooled to 12 K, results in a very steep intensity drop from 114 to 118 K (Fig. 1), indicating a first-order melting transition. This is close to the triple point (116 K at 0.72 bar) and it is therefore related to melting of the bubbles containing krypton at a fairly low pressure. It coincides with the disappearance of the skewness in the diffraction peak, where only the Gaussian distribution from the high-pressurized, small

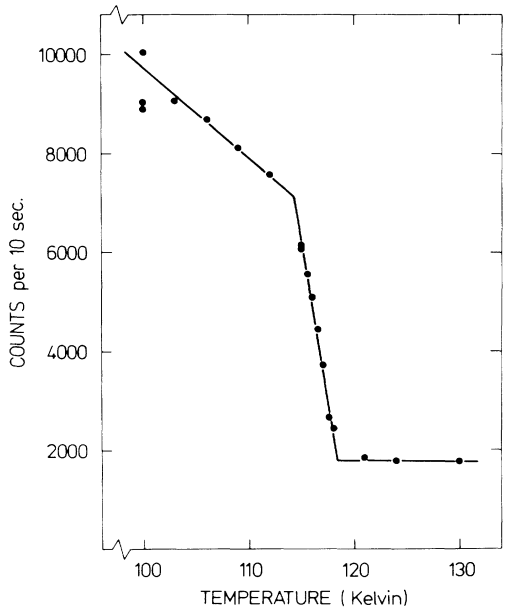

FIG. 1. The peak intensity of the ⟨111⟩ krypton peak as a function of temperature in the vicinity of the pressure-broadened melting transition at 114–118 K.

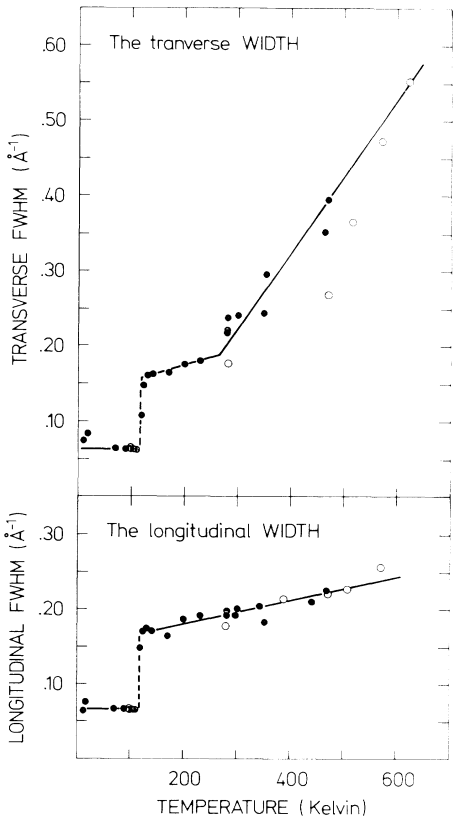

FIG. 2. The transverse and longitudinal widths of the krypton ⟨111⟩ peak as functions of temperature. Open circles are from the first anneal to 620 K of the as-implanted crystal. Filled circles are from subsequent heating and cooling cycles. The lines are guides to the eyes.

and still solid bubbles is retained. The broadening of the melting transition is a consequence of the melting occurring at constant volume. It indicates that the krypton fills out the entire volume of the bubbles, and it is consistent with the observation that annealing to 620 K causes only insignificant growth of the larger bubbles.[8]

If we use Ronchi's pressure-temperature analysis for krypton,[14] the pressure in the bubbles can be assessed from the lattice-parameter determinations. When we compare these results with the Simon equation which relates melting pressure and temperature,[15] the small bubbles $\simeq 3.5$ nm in size, retained after melting of the larger-bubble fraction at $\simeq 116$ K, are found to remain solid at least upon heating up to 620 K. Although the peak intensity decreases with increasing temperature, the integrated intensity is nearly constant. Figure 2 shows the transverse and longitudinal widths measured perpendicular and parallel to the scattering vector, respectively, as functions of temperature. The steep increase in both widths at 116 K coincides with the melting of the larger-bubble fraction and the disappearance of the skewness in the diffraction profiles. The deconvoluted width of the smaller-sized bubbles shows no discontinuity at $\simeq 116$ K. At $\simeq 300$ K the transverse profile starts to become much broader than the longitudinal one. This is not due to a gradual melting of the bubbles; in that case the integrated intensity would be reduced, which is found not to be the case. The broadening is rather interpreted as a gradual loss in orientational alignment of the still solid bubbles, induced by a roughening transition taking place on the aluminum matrix cavity surfaces.[16] At $\simeq 620$ K the diffraction pattern has evolved into a partial ring. The FWHM of a rocking scan through the Kr ⟨111⟩ peak was 16° while the longitudinal width was essentially unchanged and still corresponded to a correlation length of 2.5–3.5 nm. In electron diffraction from as-implanted samples, sharp streaks through the ⟨111⟩ diffraction spots indicate that the bubbles have {111} facets.[11] This favors a fully incoherent interface model. Prior to the roughening transition temperature, the cavities will develop towards a more spherical shape. The facets will be lost and the bubbles will gradually lose their orientational alignment with the cavity surfaces, and hence with the aluminum matrix. From a diffraction point of view the bubbles will get a larger and larger mosaic spread, causing an increase in the transverse width but not in the longitudinal width. Finally, around 620 K the transverse width is so large that the longitudinal peak becomes too small to be distinguished from the thermal background. Had the melting taken place gradually up to 620 K, the diffraction pattern would have been composed of a Bragg peak and a diffraction ring, resulting in a gradual loss of integrated

intensity in the Bragg peak. The open circles in Fig. 2 are from the first annealing of the as-implanted crystal. In that case, the transverse width increases more slowly with temperature at the beginning of the anneal, and the roughening is less pronounced. This may be due to the fact that, as shown in the channeling results below, large amounts of radiation damage still remain in the aluminum lattice.

Up to $\simeq$250 K the lattice parameter for the solid-bubble fraction is 0.573 nm. At higher temperatures, i.e., above the roughening, the lattice parameter decreases linearly with temperature to a value of 0.547 nm at 500 K corresponding to a pressure of 2.0 GPa. After the roughening, the attachment of the solid krypton bubbles to the aluminum cavities is reduced, and the fraction of free volume at the interface increases. Therefore, as the cavities have constant volume, the volume available for the krypton will decrease, the particles will be compressed, and the lattice parameter reduced. This additional pressure increase induced by heating may be the primary reason for retention of the solid phase up to temperatures where the bubbles start to grow. We do not see any effect of superheating as had earlier been reported by Rossouw and Donnelly.[17] However, in their electron diffraction analysis, which was carried out on polycrystalline samples, it may be difficult to distinguish the pressure-induced delayed melting of the bubbles and the gradual loss of peak intensity due to the roughening phenomenon from effects which might be ascribed to superheating.

⟨110⟩ crystals for Rutherford backscattering and channeling analysis[18] were implanted with krypton in a random direction under the same conditions as for the ⟨111⟩ crystals used for x-ray–diffraction analysis. Angular scans taken at low temperature show that the χ_{min} value for aluminum in the as-implanted crystals is 0.20. Upon annealing to 550 K this value is reduced to 0.15, showing recovery of the aluminum matrix. Channeling in the krypton particles, which is indicated by the FWHM of the dip being substantially broader than for channeling in the aluminum matrix, is not nearly as pronounced (Fig. 3). The solid circles are from an as-implanted sample after it has been cooled to 30 K. They show a linear scan from the ⟨110⟩ axis into a {110} plane. The central peak originates from krypton located in interstitial positions, and the disappearance of that signal upon the tilting into the {110} plane indicates that the interstitial positions have octahedral symmetry. The crosses in Fig. 3 are from a full circular scan measured after an annealing to 550 K and subsequent cooling to 48 K where all krypton particles are solid. The disappearance of the ⟨110⟩ axial peak shows that the interstitial-krypton fraction has disappeared by diffusion either to the surface or to the bubbles. This agrees with the results of Birtcher and Jäger who have observed a first stage in gas-release experiments around 500–600 K, which they interpreted as originating from isolated krypton atoms.[8] If we extrapolate the linear scan in Fig. 3 from the {110} plane onto the axis, the interstitial krypton fraction is estimated to contain 10%–15% of the implanted atoms.

The poor channeling properties of the solid krypton inclusions are somewhat surprising from the point of view that the inclusions are epitaxially aligned with the aluminum matrix. The x-ray–diffraction data indicate that the krypton crystals are perfect throughout, up to the incoherent interface. The near absence of channeling is

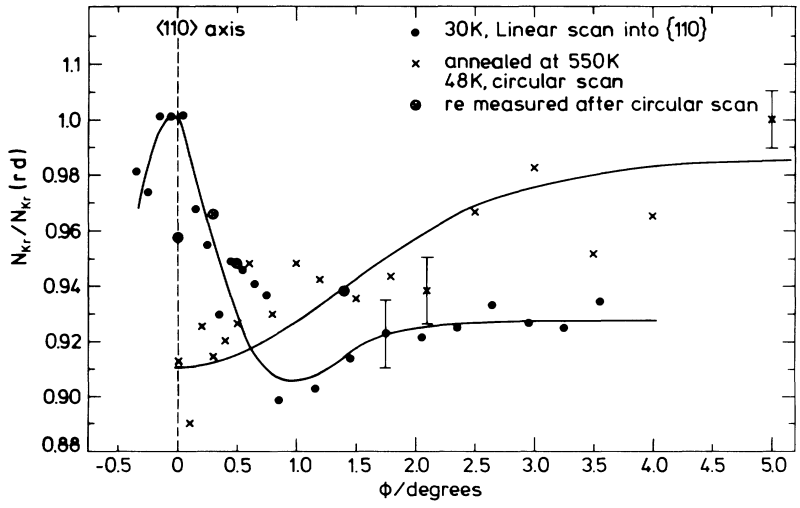

FIG. 3. Angular scans of the Rutherford-backscattering channeling krypton spectra, with the axial peak originating from an interstitial fraction of krypton atoms in the as-implanted crystal. The relatively high values of the points remeasured after the circular scan indicate a certain degree of radiation damage in the krypton crystals induced by the analyzing beam.

therefore presumably due to a gradual, systematic, and possibly even catastrophic strain-induced dechanneling, as reported earlier for strained-layer superlattices.[19] Dechanneling will take place not only at the Al/Kr interface, but also in the highly strained aluminum matrix, where the high pressure in the krypton bubbles will induce a dilatory expansion of the aluminum lattice and a gradual bending of the lattice planes in the vicinity of the bubbles.

In conclusion, we have found x-ray diffraction to be a powerful technique for obtaining quantitative information on solid inert-gas inclusions in metals. Supplemented with channeling analyses on single crystals, the two techniques yield information which is inaccessible by transmission electron microscopy. We have, in particular, analyzed the shapes of the diffraction peaks, and from determinations of their positions and their longitudinal and transverse widths we have obtained values for the lattice parameters and bubble sizes for two separate bubble fractions. The larger bubbles melt in a first-order pressure-broadened transition at 114–118 K, while the smaller bubbles under high pressure remain solid up to 600 K. As a result of the onset of roughening on the aluminum facets at $\simeq$300 K the bubbles gradually lose their alignment with the aluminum matrix. The epitaxial growth of the krypton inclusions in the aluminum matrix is thus related to the crystal morphology of both the krypton crystallites and the aluminum cavities. Then, when this morphology is lost (the roughening occurs), the epitaxial alignment is also lost. This interpretation, that the free energy is minimized when the two morphologies match, also explains why the krypton inclusions have hcp structure in an hcp matrix.[9]

We would like to thank Dr. B. Bech Nielsen, Århus University, for provision of beam time and assistance with the Rutherford-backscattering analyses. The rotating-anode source at Risø National Laboratory is funded in part by The Danish Natural Sciences Research Council.

[a]Permanent address: Minsk Radioengineering Institute, 6 Brovka St., 220069 Minsk, U.S.S.R.

[1]A. vom Felde, J. Fink, Th. Müller-Heinzerling, J. Pflüger, B. Scheerer, G. Linker, and D. Kaletta, Phys. Rev. Lett. **53**, 922 (1984).

[2]C. Templier, C. Jaouen, J. P. Riviere, J. Delafond, and J. Grilhe, C. R. Acad. Sci. Ser. 2 **299**, 613 (1984).

[3]J. H. Evans and D. J. Mazey, Scripta Metal. **19**, 621 (1985).

[4]R. C. Birtcher and W. Jäger, J. Nucl. Mater. **135**, 274 (1985).

[5]C. Templier, R. J. Gaboriaud, and H. Garem, Mater. Sci. Eng. **69**, 63 (1985).

[6]J. H. Evans and D. J. Mazey, J. Phys. F **15**, L1 (1985).

[7]C. Templier, H. Garem, and J. P. Riviere, Philos. Mag. A **53**, 667 (1986).

[8]R. C. Birtcher and W. Jäger, Ultramicroscopy **22**, 267 (1987).

[9]J. H. Evans and D. J. Mazey, J. Nucl. Mater. **138**, 176 (1986).

[10]J. C. Desoyer, C. Templier, J. Delafond, and H. Garem, Nucl. Instrum. Methods Phys. Res., Sect. B **19/20**, 450 (1987).

[11]C. Templier, H. Garem, J. P. Riviere, and J. Delafond, Nucl. Instrum. Methods Phys. Res., Sect. B **18**, 24 (1986).

[12]R. Khanna, A. K. Tyagi, R. V. Nandedkar, and G. V. N. Rao, Scripta Metal. **20**, 181 (1986).

[13]A. K. Tyagi, R. Khanna, and G. V. N. Rao, Scripta Metal. **20**, 1245 (1986).

[14]C. Ronchi, J. Nucl. Mater. **96**, 314 (1981).

[15]P. H. Lahr and W. G. Eversole, J. Chem. Eng. Data **7**, 42 (1962).

[16]M. Wortis, in *Fundamental Problems in Statistical Mechanics VI, Proceedings of the Sixth International Summer School, Trondheim, Norway, 1984,* edited by E. G. D. Cohen (Elsevier, New York, 1985), p. 87.

[17]C. J. Rossouw and S. E. Donnelly, Phys. Rev. Lett. **55**, 2960 (1985).

[18]L. C. Feldman and J. W. Mayer, *Fundamentals of Surface and Thin Film Analysis* (North-Holland, Amsterdam, 1986).

[19]S. T. Picraux, W. K. Chu, W. R. Allen, and J. A. Ellison, Nucl. Instrum. Methods Phys. Res., Sect. B **15**, 306 (1986).